Magnetic response of nanoscale left-handed metamaterials

R. S. Penciu[1], M. Kafesaki[1,2,*], Th. Koschny[1,3], E. N. Economou[1,4], and C. M. Soukoulis[1,2,3]
[1] *Foundation for Research and Technology Hellas (FORTH), Institute of Electronic Structure and Laser (IESL), P.O. Box 1385, 71110 Heraklion, Crete, Greece*
[2] *Dept. Materials Science and Technology, University of Crete, 71003 Heraklion, Greece*
[3] *Ames Laboratory and Dept. Physics and Astronomy, Iowa State University†, Ames, Iowa 50011, USA and*
[4] *Dept. of Physics, University of Crete, 71003 Heraklion, Greece**

Using detailed simulations we investigate the magnetic response of metamaterials consisting of pairs of parallel slabs or combinations of slabs with wires (including the fishnet design) as the length-scale of the structures is reduced from mm to nm. We observe the expected saturation of the magnetic resonance frequency when the structure length-scale goes to the sub-micron regime, as well as weakening of the effective permeability resonance and reduction of the spectral width of the negative permeability region. All these results are explained by using an equivalent resistor-inductor-capacitor (RLC) circuit model, taking into account the current-connected kinetic energy of the electrons inside the metallic parts through an equivalent inductance, added to the magnetic field inductance in the unit-cell. Using this model we derive simple optimization rules for achieving optical negative permeability metamaterials of improved performance. Finally, we analyze the magnetic response of the fishnet design and we explain its superior performance regarding the high attainable magnetic resonance frequency, as well as its inferior performance regarding the width of the negative permeability region.

PACS numbers: 41.20.Jb, 42.70.Qs, 81.05.Xj, 78.67.Pt

I. INTRODUCTION

Left-handed metamaterials (LHMs), i.e. artificial composite structures with overlapping negative permittivity and permeability frequency bands giving rise to negative index of refraction[1,2], have attracted recently an exponentially increasing attention. The main reason behind this attention is mainly the novel physical phenomena associated with those materials (negative refraction, opposite phase and energy velocity, reversed Doppler effect etc), which result to new capabilities in the manipulation of electromagnetic waves. Such an important capability is the superlensing capability of LHMs[3], i.e. the ability to offer subwavelength resolution imaging, which can have important implications in many scientific, technological and every-day life areas, like imaging, microscopy, lithography, ultra-compact data storage, etc.

Since the demonstration of the first left-handed material[4], in 2000, operating in the microwave regime, many left-handed (LH) structures have been created[5–11], and important efforts for the better understanding and the optimization of those structures have taken place. Among the various efforts within the LHM research, a large part has been devoted to the extension of the frequency of operation of LHMs from the microwaves to the optical regime, where the superlensing-based applications can find an important ground for manifestation. These efforts led to metamaterials with negative permeability operating in the few THz regime already in 2004[12,13], which soon were followed by the first structures of negative permeability and/or negative index of refraction in the telecommunications regime and more recently in the lower visible regime. (For reviews of the existing research efforts on infrared (IR) and optical metamaterials see Refs.[14,15].)

While the first and most of the existing microwave LHMs are systems made of split-ring resonators[16] (SRRs, i.e. interrupted metallic rings, giving rise to resonant loop-like currents, and thus to resonant permeability involving negative permeability values) and continuous wires (leading to the negative permittivity response[17]), in most of todays high frequency LHMs the SRRs have been replaced by pairs of slabs (or stripes, or wires)[18–21] - see Fig. 1(a). Like the SRR, the slab-pair also behaves as a resonant magnetic moment element, where the magnetic moment is created by resonant currents, antiparallel in the two slabs of the pair, forming a loop-like current. In most of the experimentally realized optical slab-pair&wire structures the slabs are as wide as the corresponding unit cell side and are physically connected with the wires, leading to a design known as fishnet[22–25] (see Fig. 1(d)). Fishnet design was able to give the highest in frequency LHMs up to now[26,27].

The main reason behind the replacement of SRR by the slab-pair for the high frequency metamaterials, apart of slab-pair simplicity in fabrication (which is also a crucial parameter), is its ability to exhibit negative permeability response for incidence normal to the plain of the pair; this makes possible the demonstration of the negative permeability response with just a monolayer of slab-pairs. Indeed, up to now most of the demonstrated "magnetic" metamaterials (i.e. materials of resonant and negative permeability) and LHMs are single layers, while only few multilayer samples have been fabricated[13,28]. (Note that in the optical regime what is difficult to be achieved is the negative permeability component of a LHM, since

the negative permittivity response can be easily obtained using metals; that is why most of the existing efforts to go to the optical LHMs start from attempts to achieve structures of only negative permeability.)

Since many of the existing attempts to create high frequency magnetic metamaterials and LHMs are based on the scaling down of known microwave designs, there are already efforts trying to determine the possibilities and the limitations of this scaling approach[30–33]. (Note that the properties of the metals, which are involved in most of todays metamaterials, are drastically different in the optical regime compared to microwaves - there, metals behave almost as perfect conductors.) Most of those attempts concern SRR systems and they have led to two important conclusions[30,34,35]:

(a) By scaling down a SRR, the frequency of its resonant magnetic response does not continuously increase, but after some length scale it saturates to a constant value. This value was found to be dependent on the SRR geometry employed, and with proper modifications of this geometry (e.g., adding gaps in the SRR) it could go up to a small fraction (e.g. 20%) of the plasma frequency, i.e. to the middle visible range. The saturation response of the magnetic resonance frequency was explained taking into account the contribution of the kinetic energy of the electrons associated with the current inside the SRR ring to the magnetic energy created by the loop current (or, equivalently, taking into account the dispersive response of the metal in the conductivity).

(b) The magnetic permeability resonance becomes weaker and weaker by going to smaller length-scale SRR systems, and below some length scale it ceases to reach negative values. This weakening of the permeability was attributed to the kinetic energy of the electrons (giving rise to saturation) in combination with the increased resistive losses in the metal as one goes to higher frequencies; these losses are strengthened by the resonant response, implying long-time interaction of the wave with the metallic structures.

Although the existing studies are very revealing concerning the high frequency response of magnetic metamaterials, they examine the influence of the kinetic energy (or the dispersive response of the metals) only to the magnetic resonance frequency and not to other features of the resonant magnetic response (like resonance shape and damping factor), neither clarified the role of the losses in the saturation of the magnetic resonance frequency. Moreover, the role of the various geometrical parameters in the high frequency response of metamaterials still remains to be determined, as to identify the dominant parameters determining this response and to define optimization rules for those materials.

In this paper we attempt to study all the above mentioned issues. We will be restricted to systems based on pairs of slabs, alone or in combination with continuous wires; this is mainly due to the fact that slab-pair-based systems are offered for an easy experimental demonstration of negative permeability or negative index response

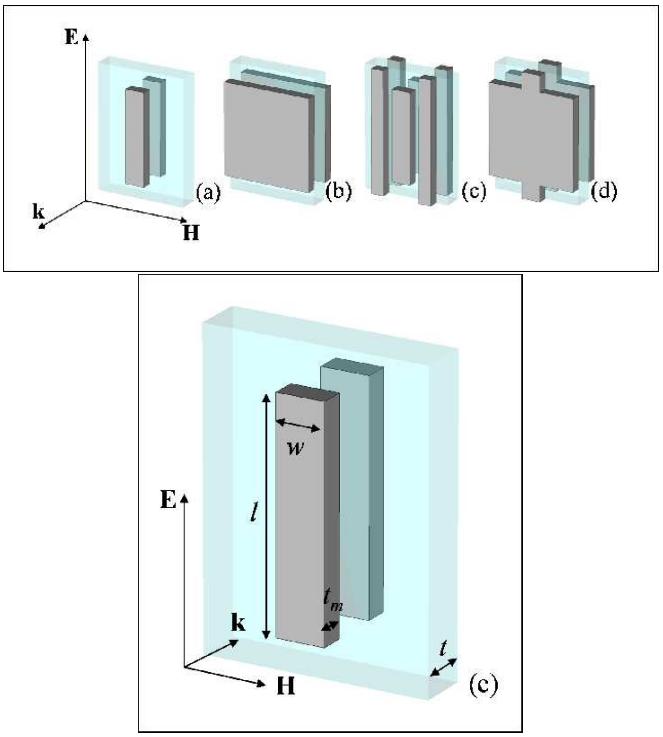

FIG. 1: The unit cell of the four designs studied. (a): Narrow-slab-pair system; (b) wide-slab-pair system; (c) slabs&wires system; (d) fishnet design. Panel (e) is a magnification of panel (a) where the structure parameters appearing in the structure simulations are shown. The parameters of the pair are given as a function of the scale parameter $a = a_{\mathbf{k}}$ (lattice constant along propagation direction; equal to the system thickness): lattice constants $a_{\mathbf{E}} = 2.97a_{\mathbf{k}}$, $a_{\mathbf{H}} = 2.19a_{\mathbf{k}}$, slab-length $l = 2.19a_{\mathbf{k}}$, slab-width $w = 0.47a_{\mathbf{k}}$, thickness of the metal $t_m = 0.25a_{\mathbf{k}}$ and thickness of the substrate $t = 0.5a_{\mathbf{k}}$. For the fishnet design (d) the width of the slabs is equal to the corresponding unit cell side ($a_{\mathbf{H}}$), while the width of the "necks" (continuous metallic parts joining the slabs along **E** direction) is $w_n = 0.469a_{\mathbf{k}}$. The dielectric spacer separating the metallic pairs has been considered as glass (with relative permittivity $\varepsilon_b = 2.14$), while for the metal plasma frequency and damping factor the aluminum parameters have been employed.

and, moreover, have been proven up to now the most promising systems for the achievement of high frequency negative permeability and negative index metamaterials. The structures discussed here are shown in Fig. 1. Following the approach of Refs.[30,35], we will attempt to analyze the high frequency magnetic response of those structures, to compare their performance and to propose optimization rules for them. For that we examine in detail the scaling behavior of the magnetic resonance frequency and the magnetic permeability as the structures are scaled down from mm to nm scale.

The basic idea that we will use to reproduce and understand the small length scale (high frequency) behavior of our structures is the consideration of the kinetic energy of the current carried electrons. This kinetic energy, as

being proportional to the square of the velocity (and thus of the frequency, just like the magnetic energy), is added to the magnetic energy of the structures and in small length-scales it dominates the magnetic metamaterials response. The consideration of this kinetic energy is done here through an equivalent "kinetic" inductance[30,36] (or electrons' inductance), added to the magnetic field inductance in an effective resistor-inductor-capacitor (RLC) description of the artificial magnetic structures.

Specifically, the paper is organized as follows: In Section II we present the "high frequency" response of our structures, as revealed by numerical simulations concerning the magnetic resonance frequency, the form of the magnetic permeability resonance and the losses. The wave propagation characteristics in those structures are analyzed and explained in Section III, using an effective RLC description of the structures and taking into account the dispersive behavior of the metals through the kinetic metal inductance. Based on the results and analysis of Sections II and III, in Section IV we present basic optimization rules for the achievement of high frequency magnetic metamaterials and left-handed materials with improved performance. There we discuss also the fishnet design, which has been proven up to now the optimum design for achievement of optical negative index materials. Finally, in Section V we show that the simple RLC circuit model does not only have qualitative power, but it can be used also to give quantitative results if plugged with accurate relations for the capacitance and the inductance of the system.

II. NUMERICAL SIMULATIONS

In this section we present calculation results concerning the scaling of the magnetic resonance frequency and the magnetic permeability of the structures shown in Fig. 1. The geometrical parameters used in the simulations are those mentioned in Fig. 1; for the permittivity of the metal the Drude dispersion model has been employed, i.e. $\varepsilon = \varepsilon_0[\varepsilon^{(0)} - \omega_p^2/(\omega^2 + i\omega\gamma_m)]$, with the parameters of the aluminum (plasma frequency $\omega_p = 22.43 \times 10^{15}$ sec^{-1}, collision frequency $\gamma_m = 12.18 \times 10^{13}$ sec^{-1}), and $\varepsilon^{(0)} = 1$. Using Drude dispersion model one takes automatically into account the mass and any kinetic energy of the current-carrying electrons inside the metal (the contribution of the bound electrons is also taken into account, through the constant $\varepsilon^{(0)}$).

The calculations presented here have been performed using the Finite Integration Technique, employed through the MicroWave Studio (MWS) commercial software. Using MWS, the transmission and reflection from a monolayer of the structure have been obtained; these data have been used for the determination of the effective permittivity and permeability of the structures, through a standard retrieval procedure based on a homogeneous effective medium approach[37,38].

In Fig. 2 we present the magnetic resonance frequency

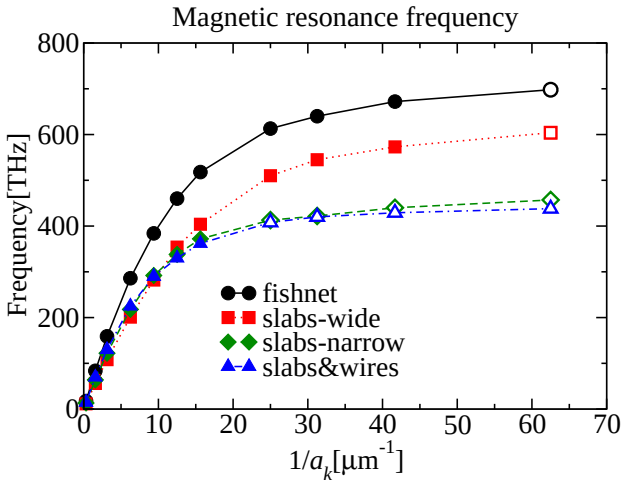

FIG. 2: Scaling of the magnetic resonance frequency with the linear size of the unit cell along propagation direction (a_k) for the four designs of Fig. 1: Fishnet (black circles), wide-slabs (red squares), narrow-slabs (green diamonds), slabs&wires (blue triangles). The solid symbols indicate the existence of negative permittivity values, while the open symbols indicate that the permeability resonance is weak and unable to reach negative values for the Re(μ).

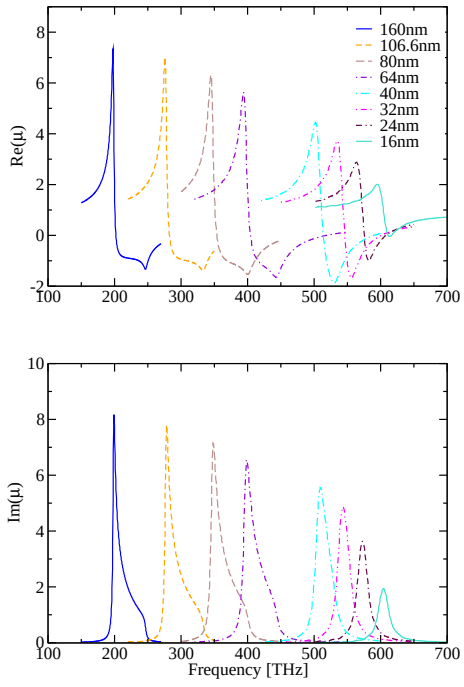

FIG. 3: Frequency dependence of the real (top panel) and the imaginary (bottom panel) part of the magnetic permeability of the wide slab-pair system for various length scales. The legends indicate the lattice constant along propagation direction for each specific system.

for the four structures of Fig. 1 as the structures are scaled down from mm to nm scale; in Fig. 3 we show the real and imaginary part of the magnetic permeability as a function of frequency, for wide-slab-pairs (structure of Fig. 1(b)) of various length scales.

As can be seen in Fig. 2, in slab-pair systems we observe the same behavior as the one reported earlier for SRR structures[30,35]: while in larger length-scales the magnetic resonance frequency scales inversely proportional to the structure linear size, at frequencies in the near infrared (IR) towards optical regime this linear scaling breaks down, and the magnetic resonance frequency saturates to a constant value. This saturation value is different for the different designs employed, with larger the one of the fishnet structure. Note that in the slabs&wires case (structure of Fig. 1(c)) the presence of wires does not affect the magnetic resonance frequency of the slabs, while in the fishnet structure the presence of wires leads to higher saturation value for the magnetic resonance frequency. This behavior of the fishnet design will be discussed and explained in Section IV.

It is important to mention here that the saturation values for the magnetic resonance frequency of the slab-pair-systems are in all cases larger than the saturation values obtained for SRRs of a single gap[39] (like, e.g., U-shaped SRRs; single-gap SRRs are the only SRR-based system that has been fabricated in the nm scale), indicating once more the suitability of the slab-pair-based systems for the achievement of optical magnetic metamaterials.

Concerning the permeability results shown in Fig. 3, we observe that, just like the SRRs[30,35], as the length scale of the structure becomes smaller the permeability resonance becomes weaker, ceasing ultimately to reach negative values. This weakening is revealed in both the real and imaginary part of the permeability resonance, and it will be analyzed in more detail and quantified in the following paragraphs. (Note that the "truncation" of the resonances of Fig. 3, which is observed in the larger scale structures, is a result of the larger influence of the periodicity in these length scales[40]. In smaller scales this influence becomes smaller, due to the deeper sub-wavelength scale of the corresponding structures and the weaker resonant response, which results to smaller effective index and thus larger wavelength inside the structures.)

One quantity which is of great interest in left-handed materials and it is strongly affected by the weakening of the permeability resonance is the width of the negative permeability regime, which roughly corresponds with the operational band width of a LHM. In Fig. 4 we present the relative band-width (i.e. band-width divided by the lower frequency of the negative permeability band) for the four structures shown in Fig. 1. As can be seen in Fig. 4, the operational band-width, which in larger scales is almost independent of the length scale, in smaller scales it is strongly reduced, ultimately going to zero for all designs. This shows that the negative permeability

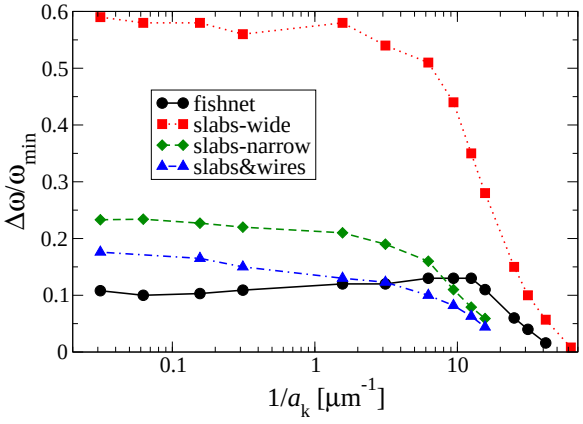

FIG. 4: Band-width, $\Delta\omega$, of the negative magnetic permeability regime vs the inverse unit cell size, $1/a_{\mathbf{k}}$, for fishnet (black circles), wide-slab-pairs (red squares), narrow-slab-pairs (green diamonds) and slabs&wires (blue triangles). The band-width is normalized by the minimum frequency (lower limit) of the negative permeability regime, $\omega_{\rm min}$. $a_{\mathbf{k}}$ is the lattice constant along propagation direction.

is ultimately killed in the nm scale structures. Among our four structures the wide-slab-pair one is characterized by the larger band-width. Finally, it is worth-noticing the reduced band-width of the fishnet design, compared to the band-width of the slab-pair-only structure. This bandwidth behavior will be discussed in the next section.

Since a main issue for the achievement of high frequency metamaterials of satisfactory performance is the losses, due to the increased resistive losses in the metallic components going to the optical regime, we performed a detailed analysis of the losses in high frequency metamaterials, trying to estimate which aspects of the high frequency metamaterial response are mainly affected by the resistive losses, and, consequently, to seek ways to minimize the influence of those losses, using proper design modifications.

As a first step we calculate the losses as a function of frequency for various length scales of our systems. In Fig. 5 we present these losses for the wide-slab-pair system of Fig. 1(b). The losses, A, have been calculated through the relation $A = 1 - R - T$, where R and T are the reflection and transmission coefficient, respectively, through one unit cell of the structure along propagation direction. As is expected, the losses show a dramatic increase by going to smaller length scales and higher frequencies. This increase seems to have an exponential dependence on the magnetic resonance frequency.

From Figs 2-5, one can see clearly the decreased performance of our structures going to nm scale, inhibiting their ability to give high quality optical left-handed metamaterials. An interesting question arising here is the role of the resistive losses on this decreased performance. To examine this role, we repeated the above shown calculations using for the metal a $2\pi \times 1000$ times reduced collision frequency compared to that of aluminum, i.e.

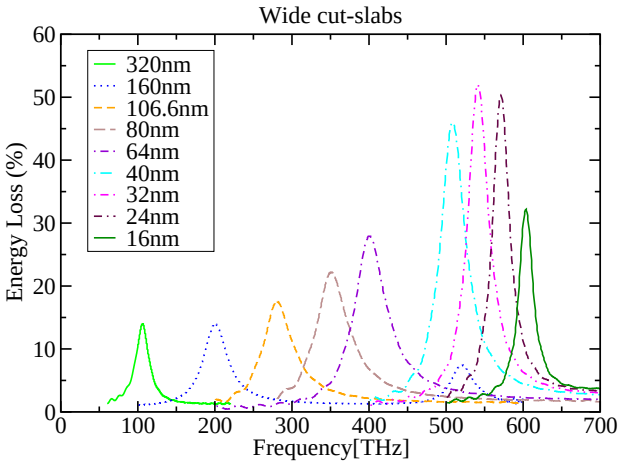

FIG. 5: Loss, A, per unit cell (%) for the wide-slab-pair system for various length scales of the system, close to the magnetic resonance frequency saturation regime. The legends indicate the lattice constant along propagation direction.

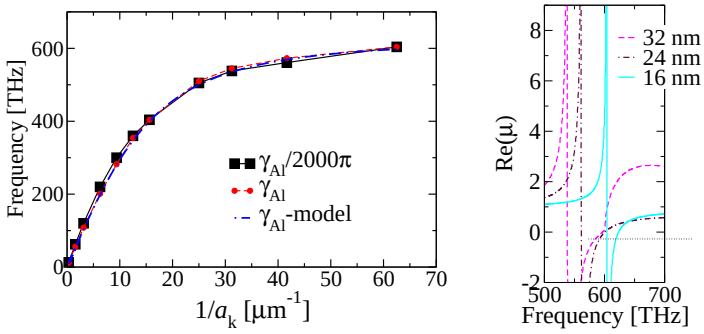

FIG. 6: (a): Saturation of the magnetic resonance frequency for the wide-slab-pair structure using for the metal a 2000π times reduced collision frequency compared with that of aluminum, i.e. $\gamma_m = \gamma_{Al}/2000\pi$ (solid-black line with squares). For comparison the corresponding result for $\gamma_m = \gamma_{Al}$ is given (dashed-red line with circles). Dotted-dashed line (blue color) shows the scaling of the magnetic resonance frequency as it is obtained from our RLC circuit model (for the γ_{Al} case). (b): Magnetic permeability resonance (shown in Re(μ)) as a function of frequency for the wide-slab-pair structure of Fig. 1(b), for $\gamma_m = \gamma_{Al}/2000\pi$ and for three different structure length-scales. Legends denote the lattice constant along propagation direction, $a_{\mathbf{k}}$.

$\gamma_m = 12.18 \times 10^{10}/2\pi$. The results concerning the wide-slab-pair system are shown in Fig. 6.

Specifically, Fig. 6(a) shows the saturation of the magnetic resonance frequency and Fig. 6(b) the real part of the resonant permeability response for the smaller length scales. Comparing the result of Fig. 6 with those for the non-reduced value of γ_m, one can see that the saturation of the magnetic resonance frequency seems to be totally unaffected by the value of the metal collision frequency. This indicates that the loss-factor of the metal employed is not able to affect the highest achievable magnetic resonance frequency of each specific design. On the other hand, the metal loss-factor can affect the minimum length scale able to give negative permeability response, as shown comparing Fig. 6(b) with Fig. 3(a). Indeed, in the small γ_m cases the magnetic permeability resonance is quite stronger, maintaining negative values up to smaller length scales. Although the strength of the resonance (as measured, e.g., by the minimum value of the Re(μ)) seems to be strongly affected by the γ_m value, calculating the width of the negative permeability regime (in the cases that such a regime exists), $\Delta\omega$ - not shown here -, it is observed that it is only slightly affected by the γ_m value; it tends to zero for both high and low values of γ_m, indicating that even in the absence of resistive losses one can not go to arbitrarily high-frequency negative permeability response over a practical band-width.

The results presented above raise many questions concerning the high-frequency magnetic metamaterial response and the main phenomena and factors determining this response. Before attempting an interpretation of this response we will summarize here the main effects observed so far and the main questions that one needs to address as to clarify and to be able to predict the existence or performance of optical negative magnetic permeability response:

(a) The magnetic resonance frequency of slab-pair-based systems, while in mm scale structures scales inversely proportional to the structure length-scale, in sub-μm scale structures saturates to a constant value, depending mainly on the geometry of the structure and independent of the resistive losses in the component materials. Among the structures that have been studied here the fishnet design leads to the higher saturation frequency. Moreover, while in the slabs&wires design the magnetic resonance frequency is almost unaffected by the presence of the wires, it is not the same in the fishnet design, where the saturation value is quite higher than the saturation value for the the slabs only case.

(b) The magnetic permeability resonance in sub-μm scale structures becomes more and more weak by reducing the structure length-scale, and ultimately ceases to reach negative values. The length scale at which $\mu < 0$ stops to exist depends on the structure geometry (design) and on the resistive losses in the component materials, especially in the metallic parts. Among the structures that we have examined, negative permeability in smaller length scales is achieved in the slab-pair structures, not associated though with higher magnetic resonance frequency. Negative permeability at higher frequencies is achieved in the fishnet design.

(c) Concerning the relative spectral width of the negative permeability regime, this width, while it is constant in mm scale structures, as one goes towards nm scales it becomes smaller and smaller, up to almost vanishing. This width depends on the structure geometry and seems only slightly dependent on the resistive metallic losses.

III. ANALYTICAL MODEL AND INTERPRETATION OF THE RESULTS

To understand and explain the results presented in the previous section, we use the common approach of describing the artificial magnetic structures (at the resonant magnetic response regime) as equivalent effective RLC circuits. Using circuit theory and basic electromagnetic considerations[2], one can easily obtain an expression for the frequency dependence of the effective magnetic permeability, $\mu(\omega)$, for a lattice of "magnetic" elements[2].

For the explanation of the high frequency magnetic response we follow the approach of Ref.[30], based on the consideration of the kinetic energy of the electrons in the metal, E_k, besides the magnetic energy of the resulting electromagnetic field. Thus, we replace the magnetic inductance of the system in the effective RLC circuit description by the total inductance resulting as a sum of the magnetic field inductance, L, and the kinetic inductance, L_e, where L_e is defined by $E_k = N_e m_e v_e^2/2 = L_e I^2/2$ (N_e is the total number of electrons, m_e is the electron mass and v_e the average electron velocity).

Assuming a slab-pair system like the one shown in Fig. 1(e), of length l and slabs separation t, excited by a magnetic field of the form $H = H_0 e^{-i\omega t}$and direction as shown in Fig. 1(e), and applying the Kirchhoff voltage rule, one can obtain

$$(L+L_e)\ddot{I} + \frac{1}{C}I + \dot{I}R = -\ddot{\phi} = \omega^2 \mu_0 l t H_0 e^{-i\omega t}. \quad (1)$$

ϕ is the external magnetic flux, $\phi = \mu_0 l t H$, and R and C the resistance (frequency independent, accounting for the ohmic losses) and the capacitance of the system, respectively. The obvious solution of Eq. (1) is $I = I_0 \mathrm{e}^{-i\omega t}$, with

$$I_0 = -\frac{\omega^2[\mu_0 l t/(L+L_e)]}{\omega^2 - 1/(L+L_e)C + i\omega R/(L+L_e)} H_0. \quad (2)$$

Having the current one can easily obtain the pair magnetic dipole moment, m = area × current = ltI, and the magnetization $M = (N_{LC}/V) ltI = (1/V_{uc}) ltI$, N_{LC} is the number of "RLC" circuits in the volume V, and $V_{uc} = a_{\mathbf{E}} a_{\mathbf{H}} a_{\mathbf{k}}$ is the volume per unit cell, where $a_{\mathbf{E}}, a_{\mathbf{H}}, a_{\mathbf{k}}$ are the system lattice constants along the $\mathbf{E}$, $\mathbf{H}$, and $\mathbf{k}$ direction respectively ($a_{\mathbf{H}} \geq w$, $a_{\mathbf{E}} > l$, $a_{\mathbf{k}} \geq t$) - see Fig. 1).

Finally, using $M = \chi_m(\omega) H, \mu(\omega)/\mu_0 = 1 + \chi_m(\omega)$, with χ_m the magnetic susceptibility, one obtains that

$$\mu(\omega) = \mu_0 [1 - \frac{(1/V_{uc})(\mu_0 (lt)^2/(L+L_e))\omega^2}{\omega^2 - \omega_{LC}^2 + i\omega\gamma}], \quad (3)$$

with

$$\omega_{LC} = \frac{1}{\sqrt{(L+L_e)C}}, \quad \gamma = \frac{R}{L+L_e}. \quad (4)$$

ω_{LC} is the magnetic resonance frequency of the system and γ is the dumping factor, representing all the losses and the scattering mechanisms.

The inductance L_e can be easily calculated by calculating the kinetic energy of the electrons, $E_k = N_e m_e v_e^2/2 = V_w n_e m_e v_e^2/2$, and expressing the velocity through the current, $I = e w t_m n_e v_e$ (n_e is the number density of free electrons, e is the electron charge, and $V_w = w t_m l$ is the volume of the metallic slab - see Fig. 1(e)). This way, one can obtain $L_e = l m_e/w t_m e^2 n_e = (l/w t_m)(1/\omega_p^2 \varepsilon_0)$, where $\omega_p = \sqrt{e^2 n_e/m_e \varepsilon_0}$ is the plasma frequency of the bulk metal.

Note that exactly the same results as in Eq. (3) can be obtained by considering, instead of the kinetic energy for the derivation of L_e, the dispersive behavior of the metal conductivity. Indeed, starting with the frequency dependent Drude-type conductivity

$$\sigma = i\varepsilon_0 \frac{\omega_p^2}{\omega + i\gamma_m}, \quad (5)$$

we obtain for the total resistance

$$R_{tot} = \frac{1}{\sigma}\frac{l}{S} = (\frac{\gamma_m}{\varepsilon_0 \omega_p^2} - i\frac{\omega}{\varepsilon_0 \omega_p^2})\frac{l}{S} = R - i\omega L_e. \quad (6)$$

Using $R_{tot} = R - i\omega L_e$ in Eq. (1) in the place of R and only the magnetic field inductance (in order to avoid counting twice the kinetic inductance L_e), one can obtain the same current solution as in Eq. (2).

In the following, to simplify our discussion we will consider the magnetic field inductance to be given by the inductance of a solenoid of area lt and length w (see Fig. 1), i.e. $L = \mu_0 lt/w$, and the capacitance by that of a parallel plate capacitor of area $wl/2$, plate separation t and dielectric core of relative dielectric constant ε_b, i.e. $C = \varepsilon_0 \varepsilon_b (wl)/t$. (Note that these formulas are appropriate for the case of wide slabs while describe much less satisfactory the narrow slabs case; in any case there is a numerical correction factor of the order of one - see also Section V. Note also that in our discussion we will not consider any inter-unit-cell capacitance[21], which is important in the case of quite long slabs, i.e. slabs that approach the unit cell boundaries along $\mathbf{E}$ direction.)

With the above considerations, the equation (3) for the magnetic permeability takes the form

$$\mu = \mu_0 [1 - \frac{F' \omega^2}{\omega^2 - \omega_{LC}^2 + i\omega\gamma}], \quad (7)$$

with

$$F' = F\frac{L}{L+L_e},\ F = \frac{ltw}{V_{uc}} = \frac{\text{inter-pair volume}}{\text{unit cell volume}}. \quad (8)$$

Using the above formulas and their behavior going to small length scales we will show in the following that one can reproduce and explain all the high frequency magnetic response of artificial magnetic structures.

For that, it is important to notice that by scaling-down the structures uniformly, i.e. all the lengths scale proportionally to a basic length a ($= a_{\mathbf{k}}$ here), both the capacitance and the magnetic inductance scale proportionally to a, while the kinetic inductance and the resistance scale proportionally to $1/a$, i.e.

$$C = \varepsilon_0 \varepsilon_b \frac{wl}{t} \sim a,\ L = \mu_0 \frac{tl}{w} \sim a,$$

$$R = \frac{\gamma_m}{\omega_p^2 \varepsilon_0} \frac{l}{w t_m} \sim \frac{1}{a}, \text{ and } L_e = \frac{l}{w t_m} \frac{1}{\omega_p^2 \varepsilon_0} \sim \frac{1}{a}. \quad (9)$$

The above formulas shows the increasingly pronounced role that kinetic inductance (also the resistance) plays in the smaller scales. Specifically, one can see that the ratio L/L_e is of the order of $40 t t_m/\lambda_p^2$, with the typical value of λ_p ($\lambda_p = 2\pi c/\omega_p$) being around 85 nm for Al and 130 for Ag[41]. Thus, for $\sqrt{t t_m}$ smaller than 100 nm the kinetic inductance, L_e, becomes appreciable and may dominate as the length scale becomes smaller and smaller.

A. Magnetic resonance frequency

Taking into account the expression for the magnetic resonance frequency in Eq. (4), in combination with Eqs. (9), it can be shown that the magnetic resonance frequency of a slab-pair system has the following scale dependence:

$$\omega_{LC} = \frac{1}{\sqrt{(L + L_e)C}} \propto \frac{1}{\sqrt{A_1 a^2 + A_2}}, \quad (10)$$

with A_1, A_2 constants (depending on the geometrical characteristics of the structure). Eq. (10) shows that as the slabs length-scale becomes smaller the magnetic resonance frequency does not continuously increase, but beyond a length-scale it saturates to a constant value. The saturation of the magnetic resonance frequency is exactly what is observed in Fig. 2, and is exclusively due to the existence of kinetic inductance (note that the resistance, R, representing the ohmic losses, does not appear in the above formula (10)). This inductance originates from the electrons inertia and represents the "difficulty" of electrons to follow high frequency motions, i.e. their difficulty to respond to high frequency fields.

Note that without the consideration of L_e the second term in the square root of Eq. (10) would not exist, leading to a linear dependence $\omega \sim 1/a$ (as occurs in microwaves and larger scales) making unable to explain the saturation behavior observed in Fig. 2. Note also that the kinetic inductance L_e does not influence the response of the structure only at the magnetic resonance regime but at all high-frequency regimes, including permittivity resonances.

Substituting Eqs. (9) in Eq. (10) and defining normalized (dimensionless) geometrical parameters, i.e. $l' = l/a$, $t' = t/a$, $t'_m = t_m/a$, one can obtain the dependence of ω_{LC} from the geometrical characteristics of the structure, as well as an expression for the saturation value, ω_{LC}^{sat}:

$$\omega_{LC} = \frac{1}{\sqrt{\frac{\varepsilon_b l'^2}{c^2} a^2 + \frac{\varepsilon_b l'^2}{t' t'_m \omega_p^2}}} \underset{a \to 0}{\longrightarrow} \omega_p \frac{\sqrt{t' t'_m}}{l' \sqrt{\varepsilon_b}} = \omega_{LC}^{\text{sat}}. \quad (11)$$

A correction to the above formula (11) can be obtained if one takes into account also the potential energy of the electrons inside the metal slabs, through an equivalent capacitance[31], $C_e = \varepsilon_0 w t_m/l$ (the capacitance of the capacitor formed inside the metal), added to the slabs capacitance, C. In this case the saturation value for the magnetic resonance frequency is found as

$$\omega_{LC}^{\text{sat}} = \frac{\omega_p}{\sqrt{\frac{\varepsilon_b l'^2}{t' t'_m} + 1}}, \quad (12)$$

showing that the absolute upper limit for the saturation frequency is not arbitrary high but it is restricted by the plasma frequency of the bulk metal.

Since in the following we will consider systems with both l'/t' and l'/t'_m larger than unity, where the simplified equation (11) is still valid, we will omit the electron potential energy in the following discussion, keeping into account though that this energy/capacitance sets a finite upper limit for the saturation value of the magnetic resonance frequency, which is the plasma frequency of the bulk metal.

B. Magnetic permeability resonance

As had been shown in Section II, by reducing the length-scale of the artificial magnetic structures the magnetic permeability resonance becomes more and more weak, unable to lead to negative μ values beyond a length scale. This weakening is revealed in both the real part of μ (where smaller absolute values of the Max[Re(μ)] and Min[Re(μ)] are observed) and the imaginary part (where smaller Max[Im(μ)], at $\omega = \omega_{LC}$, is observed) - see Fig. 3.

A detailed examination of Eq. (7) reveals that the strength of the resonance is determined from both factors γ and F'. On the other hand, the width of the negative permeability regime, $\Delta\omega$, seems to be much more sensitive to the factor F', and almost unaffected from γ (γ has only small influence on the lower limit of the negative permeability band, while F' strongly affects the upper limit of this band). Note that in the absence of losses, i.e. $\gamma = 0$, the upper limit of the negative permeability band is $\omega_{LC}/\sqrt{1 - F'}$; the lower limit is simply ω_{LC}, i.e.

$$\Delta\omega = \omega_{LC} \left(\frac{1}{\sqrt{1 - F'}} - 1 \right). \quad (13)$$

Using Eqs. (8) and (4) in combination with with Eqs. (9), one can obtain the scaling dependence of both F' and γ, as

$$F' = F\frac{L}{L+L_e} \propto BFa^2 \tag{14}$$

(B constant) and

$$\gamma = \frac{R}{L+L_e} \propto \frac{1}{D_1 a^2 + D_2} \tag{15}$$

(D_1, D_2 constants). From Eq. (14) one can derive two important conclusions: (a) The factor F', which mainly determines the frequency width of the negative permeability regime, is independent of the resistance, R, thus independent of any loss mechanisms. (b) With the consideration of the kinetic inductance the factor F' from scale independent (if L_e is negligible) becomes scale dependent and tends to zero as the size of the structure becomes smaller and smaller ($a \to 0$). This means that even in the absence of ohmic losses, it would be impossible to get negative permeability values of band-width substantially larger than $(a^2/\lambda_p^2)\omega_{LC}$ in arbitrarily small length scales.

The scaling behavior of F' also implies that the relative bandwidth of the negative permeability regime, while it is maintained almost constant before the staring of the saturation (see Fig. 4), it becomes smaller and smaller deeper in the saturation regime, indicating that working before the saturation regime favors the widest bandwidth of each specific structure.

The geometrical dependence of the factor F' for the slab-pair design can be easily obtained by substituting Eqs. (9) to Eq. (14):

$$F' = F\frac{1}{1+c^2/(\omega_p^2 t_m t)} = \frac{F}{1+\lambda_p^2/[(2\pi)^2 t t_m]}. \tag{16}$$

Concerning the loss factor γ, from Eq. (15) one can see that γ increases as the length-scale decreases, justifying the higher losses in the smaller length scales. This increase though does not continue up to the smallest scales, but beyond a length-scale it approaches a saturation value. The geometrical dependence of γ for the slab-pair design is obtained analogously with that of F', as:

$$\gamma = \frac{\gamma_m}{1+(\omega_p^2/c^2)t_m t} = \frac{\gamma_m}{1+(2\pi)^2 t_m t/\lambda_p^2}. \tag{17}$$

Eq. (17) shows that the saturation value of γ is the collision frequency of the bulk metal as considered in the free-electron (Drude) description of the metal[42]. The saturation regime for γ is approached simultaneously with the magnetic resonance frequency saturation, showing that deep in the saturation regime the weakening of the resonance is not mainly the result of the ohmic losses but it is rather the result of the kinetic inductance (affecting through the factor F').

Finally, it is important to point out that both γ and F' depend not only on the "quality" (i.e. plasma frequency and damping factor) of the metal used for the fabrication of metamaterials but also on the geometrical parameters of the structures (see Eqs. (16) and (17)). This reveals the possibility to modify these factors, and thus to enhance the performance of the high frequency metamaterials, by modifying the geometry.

IV. OPTIMIZED DESIGNS

From the analytical formulas and the discussion of the previous section it becomes clear that for achievement of optimized high frequency (e.g. optical) magnetic metamaterials one should require: (a) Highest possible saturation value for the magnetic resonance frequency; (b) larger possible parameter F', determining the strength of the magnetic resonance and the width of the negative permeability regime; (c) smallest possible loss factor γ.

The general requirements for meeting the above conditions can be easily concluded based on Eqs. (10), (14) and (15). They demand: Structures of small capacitance, C; structures of small kinetic inductance L_e, compared to magnetic inductance, L; structures of low resistance, R. On the other hand, the role of the magnetic field inductance is more puzzling: while low inductance facilitates the achievement of high magnetic resonance frequency, it results to "lower-quality" resonance, i.e. weaker resonance and higher losses (compared to a higher inductance structure of the same length scale). Thus, the inductance optimization should be based on the specific requirements for the designed metamaterial.

To translate the above optimization conditions to specific geometrical and material conditions for the slab-pair-based systems we can use Eqs. (11), (16) and (17). From these equations can be concluded that optimized slab-pair-based systems are favored from structures of thick metal (high t_m) and thick separation layer between the slabs of the pair (i.e. high t - not as high though as to cancel the interaction between the slabs); also structures of wide slabs (i.e. large width w - to maximize the structure volume fraction F appearing in Eq. (16)). Moreover, high quality optical metamaterials demand metals of the highest possible plasma frequency and the lowest possible collision frequency.

The role of the slab-length is not one-way: while shorter slabs (compared to the corresponding unit cell side) facilitate high attainable magnetic resonance frequencies they lead to narrower negative permeability regime (due to reduced F in Eq. (16)), and vice versa.

Finally, we should emphasize here that for enhanced metamaterial performance one should target operation below the saturation regime, as to ensure large negative permeability width and lower losses.

A. The fishnet design

As was mentioned in the previous sections and can be easily concluded from Eq. (10), structures with reduced inductance lead to higher magnetic resonance frequencies. A structure based on slab-pairs which offers a considerable reduction in the inductance is the fishnet design - see Fig. 1(d). Studies of this design in microwaves[24] have revealed that at the magnetic resonance loop currents exist not only at the slab pair but also in the necks' part of the metallic element. This neck contribution can be taken into account in an effective LC circuit description of the structure by considering an additional inductance, due to the necks, which is in parallel with the inductance of the slabs, resulting to a reduced total inductance, $L_{\rm fishnet}$, with

$$\frac{1}{L_{\rm fishnet}}=\frac{1}{L_{\rm slabs}}+\frac{1}{L_{\rm necks}} \qquad (18)$$

($L_{\rm slabs}$ and $L_{\rm necks}$ represent the inductance of the slabs and the necks part respectively; note that the $L_{\rm slabs}$ here it is not exactly the same as that for the slab-pair-only system, due to the difference in the charge and current distribution between only-slab-pair systems and fishnet.) This reduced inductance leads to a magnetic resonance frequency

$$\omega^2_{LC,\,\rm fishnet}=\frac{1}{L_{\rm fishnet}C}\approx\omega^2_{LC,\,\rm slabs}(1+\frac{L_{\rm slabs}}{L_{\rm necks}}), \qquad (19)$$

i.e. higher than that of only the slabs.

By reducing the size of the structure down to submicron and nanometer scale, the inductance of both the slabs and the necks part gets a contribution from the kinetic (electrons) inductance. This contribution though does not modify the general relation (19), indicating the higher magnetic resonance frequency of the fishnet design than that of the component wide-slab-pair system even in the saturation regime.

This higher attainable magnetic resonance frequency makes the fishnet design the preferential one for the achievement of optical metamaterials, something that has been already revealed from many existing experimental and theoretical works concerning optical metamaterials[14,15].

The relation (19), combined with Eqs. (9), can easily lead to a relation for the geometrical dependence of the magnetic resonance frequency for the fishnet, i.e.

$$\omega^2_{LC,\,\rm fishnet}=\omega^2_{LC,\,\rm slabs}(1+\frac{w_n}{w}\frac{l}{a_{\mathbf{E}}-l}), \qquad (20)$$

and thus for the saturation value of this magnetic resonance frequency. In Eq. (20) w_n and w is the width of the neck and slab parts respectively (along **H**-direction) and $a_{\mathbf{E}}$ is the lattice constant along the **E** direction (see Fig. 1). Eq. (20) suggests that for the achievement of high magnetic resonance frequency saturation values for fishnet, apart from the conditions for the optimization of the slab-pair components one should pursue also wide neck parts; moreover, the wider the neck parts the higher the saturation value of the fishnet magnetic resonance frequency is.

Concerning the magnetic permeability expression for the fishnet, here the situation is more complicated compared to only-slabs systems, due to the more complicated current picture at the magnetic resonance[24]. Following the observations and conclusions of Ref.[24], according to which the fishnet unit cell can be approximated with an RLC circuit with inductance of slabs and inductance of necks connected in parallel, the magnetic permeability for the fishnet can be calculated following the same steps as the ones presented in the previous section for the slab case, with modifications in the incident flux, the magnetic moment and the total inductance per unit cell:

Here the incident flux, ϕ, can be written as $\phi=\mu_0 a_{\mathbf{E}} t H_0 {\rm e}^{-i\omega t}$, and the modified magnetic moment as

$$m=I_{\rm slabs}lt-I_{\rm necks}(a_E-l)t=IL_{\rm fishnet}[\frac{lt}{L_{\rm slabs}}-\frac{(a_{\mathbf{E}}-l)t}{L_{\rm necks}}], \qquad (21)$$

where $I=I_{\rm slabs}+I_{\rm necks}$ and $IL_{\rm fishnet}=I_{\rm slabs}L_{\rm slabs}=I_{\rm necks}L_{\rm necks}$.

The inductances $L_{\rm slabs}$ and $L_{\rm necks}$ include both the magnetic field inductance and the electrons inductance for slabs and necks.

From Eq. (21) one can see already that the presence of the necks weakens the magnetic response of the structure, since the neck contribution in the magnetic moment opposes that of the slabs.

With the above considerations, the magnetic permeability for the fishnet design can be expressed as

$$\mu(\omega)=\mu_0[1-\frac{(1/V_{uc})\mu_0 a_E t\omega^2(lt/L_{\rm slabs}-(a_E-l)t/L_{\rm necks})}{\omega^2-1/L_{\rm fishnet}C+i\omega R/L_{\rm fishnet}}]. \qquad (22)$$

Comparing the above equation with Eq. (3), one can observe that the factor multiplying the ω^2 in the numerator, which is the main factor determining the spectral width of the negative permeability regime, becomes smaller than that of the slab only case (F'). This can explain the reduced (compared to only slabs) spectral width of the fishnet negative μ regime observed in Fig. 4.

V. OBTAINING QUANTITATIVE RESULTS

In the previous sections we presented a simple RLC circuit model for obtaining qualitative results and optimizing the slab-pair-based metamaterial structures. It is important to note though that the relations (3)-(4) do not only have a qualitative power, but they can be used also to obtain quantitative results, if plugged with more accurate expressions for the capacitances and inductances involved.

Here we will demonstrate this quantitative power of our relations in the case of the wide-slab-pair system. For wide-slab-pair systems ($w = a_{\mathbf{H}}$) and examining the fields and currents at the magnetic resonance frequency, one can use for the total capacitance of the system the capacitance of two identical parallel plate capacitors connected in-series, each of capacitance $C = \epsilon_0\epsilon_b(w/t)(l/2.5)$, and for the electrons inductance the same relation as in Eq. (9), multiplied by 2 (to take into account both slabs of the pair).

The calculated magnetic resonance frequency obtained by using these relations is shown with the dotted-dashed line in Fig. 6, and as can be seen there it is in excellent agreement with the magnetic resonance frequency obtained through realistic calculations.

Using the same equations for the case of narrow slabs, one can see that they fail to describe accurately the scaling of the magnetic resonance frequency. In fact these equations predict no dependence of ω_m on the width of the slabs, unlike the observed in Fig. 2 result, which shows lower magnetic resonance frequency for the narrower slabs.

To explain this discrepancy, we should point out that as the slabs become narrower Eqs. (9) for the capacitance and the magnetic field inductance become less and less accurate, and in the limit of $w < t$ they should be replaced by the corresponding expressions for parallel wire systems, i.e. $L = \mu_0 l \ln(t/w)/\pi$, and $C = \epsilon_b\epsilon_0\pi(l/2.5)/\ln(t/w)$. The last relations for L and C lead to lower magnetic resonance frequency saturation values compared to the ones predicted by the corresponding Eqs. (9), in agreement with the numerical results presented in Fig. 2.

VI. CONCLUSIONS

In this paper we examine the magnetic response of resonant magnetic structures based on the slab-pair design, as the structures are scaled down from mm to nm scale. This response is examined using detailed numerical simulations for obtaining the frequency dependence of the magnetic permeability (including its resonant behavior) through reflection and tranmission data of realistic structures. It is observed, as expected, that the magnetic resonance frequency of the structures, while it scales inversely proportional to the structure length scale in the mm scale, it saturates to a constant value in the nano regime. This behavior depends on the design and it is independent of any ohmic losses in the structure. Among our designs, higher saturation value is observed for the fishnet design.

The permeability resonance becomes weaker and weaker as we go deeper into sub-μm scale, and ultimately it does not reach negative values. The relative spectral width of the negative permeability regime which in larger scales is almost scale independent, in sub-μm scales it becomes smaller and smaller, approaching zero, and it has very slight dependence on the ohmic losses, while it shows strong dependence on the design, being quite narrow for the fishnet design.

All the above results are explained through a simple RLC circuit model; in the inductance, L, the current-connected kinetic energy of the electrons is taken into account besides the magnetic field energy. This model is capable to determine optimization conditions for our structures, as to attain high magnetic resonance frequencies maintaining strong resonant response with a negative permeability region as wide as possible. The model explains also the superior performance of the fishnet design regarding high magnetic resonance frequency and its reduced performance regarding the width of the negative permeability region. Finally, we show that our simple RLC circuit model is capable not only to predict qualitatively the behavior of our structures, but also to give quantitative results if it is accompanied by accurate formulas for the capacitance and inductance of the systems.

VII. ACKNOWLEDGMENTS

Authors would like to acknowledge financial support by the European Union FP7 projects PHOME, ENSEMBLE, ECONAM, NIMNIL, and the COST Actions MP0702, MP0803, by the European Office of Aerospace Research and Development (under project FENIM), and by the US Department of Energy (contract no. DE-AC02-07-CH11358).

* Electronic address: kafesaki@iesl.forth.gr

[1] V. G. Veselago, Sov. Phys. Usp. **10**, 509-514 (1968).
[2] For reviews see C. M. Soukoulis, M. Kafesaki and E. N. Economou, Adv. Mater. **18**, 1941 (2006); J. B. Pendry, D. R. Smith, Phys. Today, June 2004, **37** (2004).
[3] J. B. Pendry, Phys. Rev. Lett. **85**, 3966 (2000).
[4] D. R. Smith, Willie J. Padilla, D. C. Vier, S. C. Nemat-Nasser and S. Schultz, Phys. Rev. Lett. **84**, 4184 (2000).
[5] K. Aydin, K. Guven, M. Kafesaki, L. Zhang, C. M. Soukoulis, E. Ozbay**,** Opt. Lett. **29**, 2623 (2004).
[6] R. Shelby, D. R. Smith and S. Schultz, Science **292**, 77 (2001).
[7] N. Katsarakis, T. Koschny, M. Kafesaki, E. N. Economou, E. Ozbay and C. M. Soukoulis, Phys. Rev. B **70**, 201101(R) (2004).
[8] E. Ozbay, Zh. Li, and K. Aydin, J. Phys.: Cond. Matt. **20**, 304216 (2008).
[9] K. Aydin, Zh. Li, L. Sahin, and E. Ozbay, Opt. Expr. **16**, 8835 (2008). E. Ozbay, and K. Aydin, Photon. and Nanostruct. **6**, 108 (2008).
[10] W. J. Padilla, D. N. Basov, D. R. Smith, Materials Today **9**, 28 (2006).

[11] D. R. Smith, J. B. Pendry, M. C. K. Wiltshire, Science **305**, 788 (2004).
[12] T. J. Yen *et al.*, Science **303**, 1494 (2004).
[13] N. Katsarakis *et al.*, Opt. Lett. **30**, 1348 (2005).
[14] C. M. Soukoulis, S. Linden, and M. Wegener, Science **315**, 47 (2007).
[15] V. M. Shalaev, Nat. Photon. **1**, 41 (2007).
[16] J. B. Pendry, A. Holden, D. Robbins, and W. Stewart, IEEE Trans. Microwave Theory Tech. **47**, 2075 (1999).
[17] J. B. Pendry, A. T. Holden, W.J. Stewart and I. Youngs, Phys. Rev. Lett. **76**, 4773 (1996); J. B. Pendry, A. J. Holden, D. J. Robbins, and W. J. Stewart, J. Phys. Cond. Matt. **10**, 4785 (1998).
[18] V. A. Podolskiy, A. K. Sarychev, and V. M. Shalaev, Opt. Expr. **11**, 735 (2003).
[19] V. M. Shalaev, W. Cai, U.K. Chettiar, H.-K. Yuan, A.K. Sarychev, V.P. Drachev, and A.V. Kildishev, Opt. Lett. **30**, 3356 (2005).
[20] G. Dolling, C. Enkrich, M. Wegener, S. Linden, J. Zhou, and C. M. Soukoulis, Opt. Lett. **30**, 3198 (2005).
[21] J. Zhou, E. N. Economou, Th. Koschny, and C. M. Soukoulis, Opt. Lett. **31**, 3620 (2006).
[22] S. Zhang, et al., Phys. Rev. Lett. **95**, 137404 (2005); S. Zhang, et al., Phys. Rev. Lett. **94**, 037402 (2005).
[23] R. Ulrich, Infrared Phys. **7**, 37 (1967).
[24] M. Kafesaki, I. Tsiapa, N. Katsarakis, Th. Koschny, C. M. Soukoulis and E. N. Economou, Phys. Rev. B **75**, 235114 (2007).
[25] C. Helgert, C. Menzel, C. Rockstuhl, E. P. Severin, E. B. Kley, A. Chipouline, A. Tunnermann, F. Lederer and T. Pertsch, Opt. Lett. **34**, 704 (2009).
[26] U. K. Chettiar, A. V. Kildishev, H.-K. Yuan, W. Cai, S. Xiao, V. P. Drachev, and V. M. Shalaev, Opt. Lett. **32**, 1671 (2007).
[27] G. Dolling, M. Wegener, C. M. Soukoulis, and S. Linden, Opt. Lett. **32**, 53 (2007).
[28] N. Liu, H. Liu, S. Zhu, and H. Giessen, Nat. Photon. **3**, 157 (2009).
[29] J. Valentine, S. Zhang, Th. Zentgraf, E. Ulin-Avila, D. A Genov, G. Bartal and X. Zhang, Nature **455**, 376, (2008).
[30] J. Zhou, Th. Koschny, M. Kafesaki, E. N. Economou, J. B. Pendry, and C. M. Soukoulis, Phys. Rev. Lett. **95**, 223902 (2005).
[31] S. Tretyakov, Metamaterials **1**, 40 (2007)
[32] A. Ishikawa, T. Tanaka, S. Kawata, J. Opt. Soc. Am. B **24**, 510 (2007).
[33] A. K. Sarychev, G. Shvets, and V. M. Shalaev, Phys Rev E **73**, 036609 (2006).
[34] E. N. Economou, C. M. Soukoulis, M. Kafesaki, to appear JTCN
[35] M. Soukoulis, Th. Koschny, J. Zhou, M. Kafesaki, E. N. Economou, Phys. Stat. Sol. (b) **244**, 1181 (2007).
[36] L. Solymar, Lectures on Electromagnetic Theory (Oxford University Press, Oxford, 1976).
[37] D. R. Smith, S. Schultz, P. Markos and C. M. Soukoulis, Phys. Rev. B **65**, 195104 (2002).
[38] D. R. Smith, D. C. Vier, Th. Koschny and C. M. Soukoulis, Phys. Rev. E **71**, 036617 (2005).
[39] M. W. Klein, C. Enkrich, M. Wegener, C. M. Soukoulis and S. Linden, Opt. Lett. **31**, 1259 (2006).
[40] T. Koschny, P. Markos, D. R. Smith and C. M. Soukoulis, Phys. Rev. E **68**, 065602(R) (2003); Th. Koschny, P. Markos, E. N. Economou, D. R. Smith, D. C. Vier and C. M. Soukoulis, Phys. Rev. B **71**, 245105 (2005).
[41] P. R. West, S. Ishii, G. Naik, N. Emani, V. M. Shalaev, and A. Boltasseva, submitted to Laser and Photonics Rev. (available at http://arxiv.org/abs/0911.2737/)
[42] Usually in simulations concerning realistic structures the factor γ employed is slightly larger than that of the bulk metal, to account for the surface scattering effects.